

University of Nebraska - Lincoln
DigitalCommons@University of Nebraska - Lincoln

CSE Journal Articles

Computer Science and Engineering, Department of

2016

Modeling Changes in Measured Conductance of Thin Boron Carbide Semiconducting Films Under Irradiation

George G. Peterson

University of Nebraska-Lincoln, gpeterson5@unl.edu

Yongqiang Wang

University of Nebraska-Lincoln

Natale J. Ianno

University of Nebraska-Lincoln, nianno1@unl.edu

Michael Nastasi

University of Nebraska-Lincoln, mnastasi2@unl.edu

Follow this and additional works at: <http://digitalcommons.unl.edu/csearticles>

Peterson, George G.; Wang, Yongqiang; Ianno, Natale J.; and Nastasi, Michael, "Modeling Changes in Measured Conductance of Thin Boron Carbide Semiconducting Films Under Irradiation" (2016). *CSE Journal Articles*. 139.
<http://digitalcommons.unl.edu/csearticles/139>

This Article is brought to you for free and open access by the Computer Science and Engineering, Department of at DigitalCommons@University of Nebraska - Lincoln. It has been accepted for inclusion in CSE Journal Articles by an authorized administrator of DigitalCommons@University of Nebraska - Lincoln.

Modeling Changes in Measured Conductance of Thin Boron Carbide Semiconducting Films Under Irradiation

George G. Peterson, Yongqiang Wang, N. J. Ianno, and Michael Nastasi

Abstract— Semiconducting, p-type, amorphous partially dehydrogenated boron carbide films ($a\text{-B}_{10}\text{C}_{2+x}\text{:H}_y$) were deposited utilizing plasma enhanced chemical vapor deposition (PECVD) onto n-type silicon thus creating a heterojunction diode. A model was developed for the conductance of the device as a function of perturbation frequency (f) that incorporates changes of the electrical properties for both the $a\text{-B}_{10}\text{C}_{2+x}\text{:H}_y$ film and the silicon substrate when irradiated. The virgin model has 3 independent variables (R1, C1, R3), and 1 dependent variable (f). Samples were then irradiated with 200 keV He^+ ions, and the conductance model was matched to the measured data. It was found that initial irradiation (0.1 displacements per atom (dpa) equivalent) resulted in a decrease in the parallel junction resistance parameter from 6032 Ω to 2705 Ω . Further irradiation drastically increased the parallel junction resistance parameter to 39000 Ω (0.2 dpa equivalent), 77440 Ω (0.3 dpa equivalent), and 190000 Ω (0.5 dpa equivalent). It is believed that the initial irradiation causes type inversion of the silicon substrate changing the original junction from a p-n to a p-p⁺ with a much lower barrier height leading to a lower junction resistance component between the $a\text{-B}_{10}\text{C}_{2+x}\text{:H}_y$ and irradiated silicon. Additionally, it was found that after irradiation, a second parallel resistor and capacitor component is required for the model, introducing 2 additional independent variables (R2, C2). This is interpreted as the junction between the irradiated and virgin silicon near ion end of range.

Index Terms— Alpha particle radiation, Conductance, Hydrogenated boron carbides, Neutron detector, p-n heterojunction, Semiconducting boron carbides.

NOMENCLATURE

PECVD	Plasma enhanced chemical vapor deposition.
D	Dissipation factor.
G	Conductance.
G_m	Measured conductance.
G_0	Low frequency conductance.
C_p	Equivalent parallel circuit capacitance.

ω	Angular frequency ($\omega = 2\pi f$).
f	Small signal perturbation frequency.
CINT	Center for Integrated Nanotechnologies.
LANL	Los Alamos National Laboratory.
SRIM	Stopping and range of ions in matter.
DPA	Displacements per atom.
$a\text{-B}_{10}\text{C}_{2+x}\text{:H}_y$	Semiconducting amorphous partially dehydrogenated boron carbide film.
Z	Equivalent complex impedance.
Y	Complex admittance.
C1	1 st Parallel capacitance component: interpreted as $a\text{-B}_{10}\text{C}_{2+x}\text{:H}_y$ dielectric film.
R1	1 st Parallel junction resistance: interpreted as $a\text{-B}_{10}\text{C}_{2+x}\text{:H}_y/\text{Si}$ and/or $a\text{-B}_{10}\text{C}_{2+x}\text{:H}_y/\text{Cr}$ interface(s).
C2	2 nd Parallel capacitance component: interpreted as depletion region between irradiated Si/virgin Si interface.
R2	2 nd Parallel junction resistance component: interpreted as silicon p-n homojunction near ion end of range.
R3	Series resistance of device including quasi-neutral region of Si substrate, contact resistance of anode & external circuitry.
TEM	Transmission electron microscopy
V_2	Di-vacancy state.
ρ	Resistivity.
q	Elementary charge.
μ_p	Hole mobility.
N_A	Doping concentration of acceptors in a p-type film.
R	Resistance.
L	Film length.
W	Film width.
t	Film thickness.

This work was performed in part in the Nebraska Nanoscale Facility: National Nanotechnology Coordinated Infrastructure and the Nebraska Center for Materials and Nanoscience, which are supported by the National Science Foundation under Award ECCS: 1542182, and the Nebraska Research Initiative.

George Peterson and Mike Nastasi are with the Department of Mechanical and Materials Engineering, University of Nebraska-Lincoln, Lincoln, NE 68588-0526, USA.

Yongqiang Wang is with the Materials Science and Technology Division, Los Alamos National Laboratory, PO Box 1663, Los Alamos, NM 87545, USA.

N. J. Ianno is with the Department of Electrical Engineering, and the Center for Microelectronics and Optical Materials Research, University of Nebraska-Lincoln, Lincoln, NE 68588-0511, USA.

Mike Nastasi is with the Nebraska Center for Energy Sciences Research, University of Nebraska-Lincoln, Lincoln, NE 68583-0857, USA, and also with the Nebraska Center for Materials and Nanoscience, University of Nebraska, University of Nebraska-Lincoln, Lincoln, NE, 68588-0298, USA (e-mail: mnastasi2@unl.edu).

I. INTRODUCTION

SEMICONDUCTING boron carbide icosahedral materials have been the subject of investigation for solid state neutron detection [1-12] and as a neutron voltaic for some time [13,14]. A device capable of generating a current pulse from a neutron impact must be capable of tolerating any damage caused by the impact without adverse effects to device efficiency. Boron rich icosahedrals such as boron carbide [15-19], boron nitride [20,21], and boron phosphide [22,23] materials are particularly advantageous in certain situations, such as neutron detection and neutron voltaics, due to their ability to heal neutron [15], electron [19,22,23], and He⁺ ion [24] irradiation damage. There have been many structural studies of radiation on boron carbides [15,23,25-31] as hot-pressed/sintered, powdered or sputtered samples. Our previous paper [24], which showed that heterojunction device performance improved with moderate amounts of He⁺ ion irradiation, was the first to study the effects of radiation on amorphous boron carbides as an electrical device. The ramifications of the physical changes on the electrical properties of semiconducting boron carbides have not been examined.

Heterojunction diodes created from plasma enhanced chemical vapor deposition (PECVD) of *ortho*-carborane (closo-1,2 dicarbadodecaborane, C₂B₁₀H₁₂) resulting in p-type semiconducting partially dehydrogenated boron carbide on n-type silicon (100) suffer from limits in current rectification efficiency due to high defect concentrations [32] and low carrier mobilities [33]. This leads to a constant power drain through the device, inefficient charge collection, and low sensitivity as a neutron detector or low efficiency as a neutron voltaic. These intrinsic properties of PECVD semiconducting partially dehydrogenated boron carbide on silicon p-n heterojunction diodes may be improved as degraded icosahedral structures (icosahedral carborane molecules, B₁₀C₂H₁₂, missing B and H atoms) heal under neutron, electron, and He⁺ ion irradiation. If the defect concentration is reduced, and the charge carrier mobility is increased with irradiation, this could lead to a much more efficient device the longer the device is in service, even in extremely radiation harsh environments.

Boron based thermal neutron detectors and neutron voltaics are capable of operation due to a capture-fragmentation-emission process with daughter fragment particles ⁷Li, He⁺, with large translational energy. The energetic ⁷Li and alpha fragments deposit energy in the semiconducting partially dehydrogenated boron carbide and the silicon substrate. There are 2 main means of energy deposition. The first is due to electronic stopping (ionization/excitation). The incident ion represents a sudden perturbation to the system resulting in a transfer of energy from the projectile to the electrons of the target material [35] which can lead to bond breaking. The second form of deposition is due to energy transfer through the elastic collisions (recoil) between the projectile ion and the atoms of the target material. This energy deposition can result in atomic displacements, ultimately leading to damage accumulation.

One of the more common ways to characterize a

semiconductor device is through capacitance vs frequency and capacitance vs voltage measurements with a small ac perturbation signal imposed across the device under test in a 4-point parallel circuit utilizing an impedance analyzer. This works well for devices with efficient charge separation and negligible conductance. However, if the device is highly trapped, or has a high defect concentration, the contributions to the capacitor charging current are no longer negligible. These so-called “leaky diodes” are not always accurately characterized using the capacitance measurements mentioned above because their dissipation factor (D) becomes excessive

$$D = G/(\omega C_p) \quad (1)$$

where G is conductance, ω is angular frequency ($\omega=2\pi f$), f is small signal perturbation frequency, and C_p is equivalent parallel circuit capacitance. In the case of a large dissipation factor ($D > 10$), a more suitable measurement is conductance vs frequency or conductance vs voltage. This paper seeks to determine the conductance as a function of frequency, and compare the calculated values to experimental data to examine changes in the electrical properties of the semiconducting partially dehydrogenated boron carbide as a function of radiation. For reference, the dc current vs voltage ($I(V)$) curves as a function of irradiation have been included as Appendix A, and are reprinted with permission (License Number 3961511243923) [24].

II. EXPERIMENTAL DETAILS

Device fabrication begins with an n-type silicon (P doped) substrate (100) with resistivity of 1-10 $\Omega \times \text{cm}$ (purchased from Silicon Inc., Boise, ID). Substrates are cleaned in sequential baths of acetone, methanol, de-ionized water, and 5 wt% hydrofluoric acid for hydrogen termination [36]. The semiconducting amorphous partially dehydrogenated boron carbide films are synthesized via plasma enhanced chemical vapor deposition (PECVD) utilizing *ortho*-carborane (closo-1,2 dicarbadodecaborane, C₂B₁₀H₁₂) as the precursor (purchased from Sigma Aldrich). Details of the deposition process were previously reported [24,37]. The reported stoichiometric compositions of semiconducting amorphous partially dehydrogenated boron carbide films have varied widely [8,38,39]. This is represented by a-B₁₀C_{2+x}H_y with $0 < x < 3$ and $0 < y < 12$. For this study, according to elastic recoil detection measurements, x is approximately 0, and y is approximately 4.

Irradiation was completed at the Center for Integrated Nanotechnologies (CINT), within Los Alamos National Laboratory (LANL) using a 200 kV Danfysik implanter. 200 keV He⁺ ions were implanted to a fluence of 6.5×10^{16} ions/cm² with the He⁺ ion beam current density of $\sim 4.4 \mu\text{A}/\text{cm}^2$. Air-cooling was applied to ensure that the sample temperature remained below 40° C during irradiation.

As previously reported [24], through the application of the Monte Carlo SRIM simulation (stopping and range of ions in matter code) [35] an ion range of ~ 1400 nm was projected for

200 keV He⁺ ions. Also reported [24], one aliquot of fluence (i.e. 6.5×10¹⁶ ions/cm²) was calculated to result in 0.1 displacements per atom (dpa) in the a-B₁₀C_{2+x}:H_y films studied. The fluence to dose (dpa) relationship is linear: 2 times the above fluence yields 0.2 dpa in dose, etc.

Following irradiation, the samples were returned for electrical characterization. Conductance versus frequency $G(f)$ measurements were taken using an HP model 4192A impedance analyzer with an oscillation voltage set to 0.010 v in a 4 point parallel circuit. The analyzer has 4 parallel connections. From left to right, they are: low current, low potential, high potential, high current. By creating a metal housing for the diode under test and connecting the housing directly to the analyzer through un-insulated BNC connectors, the negative portion of the 4 connections are grounded to the analyzer creating an RF shield around the diode under test. The 4192A impedance analyzer has a conductance measurement range of 1×10⁻⁹ Ω⁻¹ to 12.999 Ω⁻¹ with an accuracy of 0.1%, and a resolution of 4 ½ digits for both grounded and floated devices.

III. RESULTS

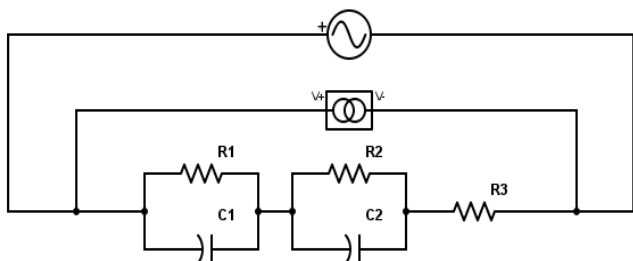


Fig. 1. Circuit model used in analysis. R1 and C1 represent the resistance and capacitance of the a-B₁₀C_{2+x}:H_y, R2 and C2 represent the resistance and capacitance of the silicon, and R3 represents series resistance.

Fig. 1 is an illustration of the circuit used to model the device under test. The small signal equivalent circuit of a p-n junction may be modeled as three parallel components comprised of the junction capacitance, diffusion capacitance, and conductance, with the junction capacitance being frequency independent [52]. C1 is interpreted as the combination of the two parallel capacitance components above due to the depletion region of the a-B₁₀C_{2+x}:H_y/Si interface. R1 is interpreted as the parallel junction resistance at the a-B₁₀C_{2+x}:H_y/Si interface. The resistance of the quasi-neutral region in the silicon substrate, metal contacts, connecting wires, and internal resistance of the analyzer are represented as the equivalent series resistance (R3). The single parallel circuit along with the equivalent series resistance suitably modeled the virgin diode. Once irradiated, this was no longer sufficient and a second RC parallel component of the circuit was found to be required. It has been shown that bulk radiation damage has a significant effect on charge carrier concentration profiles in silicon [43-49], and that single crystal silicon type-inverts from n-type to p-type at a fluence of 1.19×10¹⁴ neutrons/cm² [51], and at 1.5×10¹³ protons/cm². [54] shows that the fluence required to achieve an equivalent amount of He⁺ ion damage to 1 MeV neutrons is of

the same order of magnitude (i.e. 4.4×10¹¹ neutrons/cm² = 1×10¹¹ ions/cm²). The lowest fluence in this study was 6.5×10¹⁶ ions/cm², 2 orders of magnitude greater than reported as required for type inversion. C2 is interpreted as the junction and diffusion capacitance of the depletion region between the type-inverted irradiated silicon and virgin silicon. R2 is interpreted as the parallel junction resistance between the p-n homojunction at the irradiated silicon to virgin silicon interface.

To develop an equation for conductance as a function of frequency, an equation for equivalent complex impedance (Z) of the circuit is required. This equation plus a full derivation of the measured conductance equation is provided in Appendix B. It should be noted that while the impedance analyzer has an inductive component inherent to the machine, it was found that any inductive component was negligible in modeling the data, and is omitted from the equations. The equation describing the measured conductance G_m was found to be:

$$G_m = \frac{\omega^2((C1 R1 R2 + C2 R1 R2)(C1 R1 + C2 R2) + R3(C1 R1 + C2 R2)^2)}{\frac{\sigma_4}{(C1 C2 R1 R2 \omega^2 - 1)(-C1 C2 R1 R2 R3 \omega^2 + R1 + R2 + R3)}} \quad (2)$$

where

$$\sigma_4 = (C1 R1 R3 \omega + C2 R2 R3 \omega + C1 R1 R2 \omega + C2 R1 R2 \omega)^2 + (-C1 C2 R1 R2 R3 \omega^2 + R1 + R2 + R3)^2$$

Table I shows the results obtained for the fitting parameters of equation (2). As stated earlier, the virgin device was capable of being modeled with only the parameters of C1, R1, and R3. After moderate irradiation to 0.1 dpa, a 2nd parallel resistive (R2) and capacitive (C2) component is required. Table I shows these values to be 40 Ω and 1.166×10⁻⁹ F. Additionally, the resistance of R1 is reduced by 55.2%. Irradiation to 0.2 dpa in the a-B₁₀C_{2+x}:H_y film, results in a dramatic increase in resistance R1 of 1341.8%. Irradiation to 0.3 dpa in the a-B₁₀C_{2+x}:H_y film, results in another dramatic increase in resistance parameter R1 of 98.6%. Further irradiation to 0.5 dpa in the a-B₁₀C_{2+x}:H_y film, continues the trend of another dramatic

TABLE I
FITTING PARAMETER VALUES OF EQUATION (2)

Sample	C1 (nF)	R1 (Ω)	R3 (Ω)	C2 (nF)	R2 (Ω)	χ ²
Virgin	1.150	6082	90	0	0	0.0006360
0.1 dpa	0.8673	2782	70	1.166	40	0.0003835
0.2 dpa	0.8711	39000	70	1.617	50	0.0001278
0.3 dpa	0.7624	77440	133	0.8554	95	0.0004651
0.5 dpa	1.294	190000	65	1.752	38	0.0008379

C1 is interpreted as the capacitance due to the a-B₁₀C_{2+x}:H_y dielectric film. R2 is interpreted as the a-B₁₀C_{2+x}:H_y/Si junction resistance and a-B₁₀C_{2+x}:H_y/Cr contact resistance, C2 is interpreted as the Si(Irradiate)/Si(virgin) homojunction capacitance, R2 is interpreted as the junction resistance of the Si(Irradiate)/Si(virgin) homojunction, and R3 is interpreted as the equivalent series resistance of the device. χ² is the chi square goodness-of-fit-test statistic. A χ² value < 0.412 corresponds to a 99.5% confidence level.

increase in the resistance of parameter R1 of 145.4%.

The parameter interpreted as the equivalent series resistance of the device (R3) remains within the expected range calculated for the quasi-neutral silicon substrate of 26 to 260 Ω based on the resistivity range provided by the manufacturer. The changes of R3 listed in Table 1 are not viewed as a significant deviation. Changes in the fitting parameters C1 and C2 of tenths of a nano-farad, are not viewed as significant deviations as the device is irradiated. Changes in the parallel resistance parameter R2 follow the general pattern of R3, and are interpreted as minor changes in the carrier concentration profile inherent to the substrate rather than a result of changes due to irradiation.

When the modeled conductance is overlaid on the measured data on a linear scale, the two are nearly indistinguishable. This is indicated by the chi square goodness-of-fit-test statistics with values 3 orders of magnitude less than the value corresponding to a 99.5% confidence interval. Fig. 2 shows the measured conductance versus frequency and overlaid modeled conductance versus frequency curves on a Log-Log scale. Using the Log-Log scale, Fig. 2 shows that the low frequency conductance (G_0), is unique for each level of irradiation. Examination of Fig. 2 also shows that the frequency at which charge carriers can no longer respond to the perturbation signal (indicated by an increase in conductance) decreases as the level of irradiation damage increases. For the virgin sample, this is just above 10^4 Hz, but for the 0.5 dpa sample, there are charge carriers that cannot respond to a 10 Hz signal. The slope of the curves between 2×10^4 Hz and 1 MHz is unique to each level of irradiation. The upper limit of conductivity, as frequency approaches infinity ($f \rightarrow \infty$), consolidates into a narrow band. A difference between the virgin and irradiated samples exists.

IV. DISCUSSION

The Mathworks® Matlab curve fitting toolbox was utilized to determine the best values for the independent parameters of equation (2) (C1, R1, C2, R2, R3), as a function of the perturbation frequency utilizing bisquare weighting, which

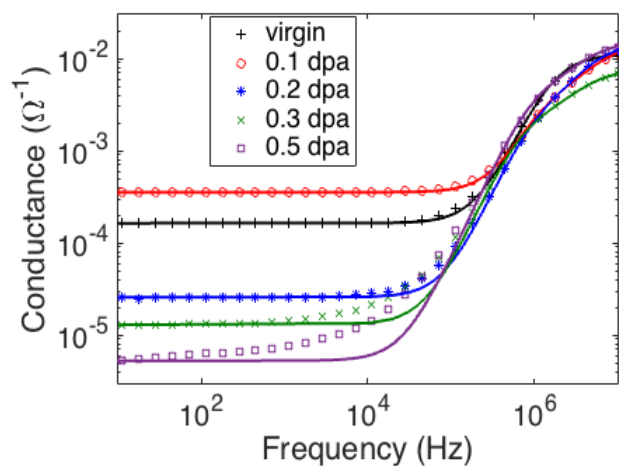


Fig. 2: Logarithmic Conductance vs. Frequency curve of a-B₁₀C_{2+x}H_y on Si heterojunctions. The black '+' represents the measured virgin data. The red 'o' represents the measured 0.1 dpa data. The blue '*' represents the measured 0.2 dpa data. The green 'x' represents the measured 0.3 dpa data. The purple '□' represents the measured 0.5 dpa data. The colored solid lines are the corresponding calculated models.

gives the strongest weighting to data points near the fit, and low weighting to outlying data points. In fitting the data to obtain the results of Table 1, parts of the model are very sensitive to specific variables of equation (2). In the low frequency range, below 10 kHz, although the limit of G_m as frequency approaches 0 ($f \rightarrow 0$) is inversely proportional to $R1 + R2 + R3$, it is only sensitive to changes in R1 (resistance of the original R1, C1 parallel component). In the high frequency range, the limit of G_m as frequency approaches infinity ($f \rightarrow \infty$) is inversely proportional to R3 (equivalent series resistance of the device). The initial upturn in conductance is dominated by C1. And the slope between the upper and lower limits of conductance is dominated by R2 and C2 (The resistance and capacitance of the 2nd parallel RC component).

The model does not fit the low frequency conductance particularly well for the samples irradiated above 0.3 dpa. Previously published TEM images [24] show a direct correlation between the SRIM calculated vacancy profile and the damage to the Si substrate as well as between He bubble formation and the SRIM calculated peak of the He distribution profile. The TEM images also provided visual evidence of point defect agglomeration. These structural changes in the Si substrate provide visual indications that di-vacancy states (V_2), formed by the combination of vacancies created in close proximity to each other, and other vacancy complexes, allow us to infer that there should be an anisotropic distribution of trap energy states available, as well as a distribution in the concentration of those states. Fig. 2 lends electronic evidence to the inferences of the visual evidence of TEM [24]. For the 0.3 dpa and 0.5 dpa samples, it is no longer the junction capacitance (which is frequency independent and is not lifetime sensitive) that dominates in the silicon, but diffusion capacitance or charging due to traps, which are frequency dependent [40]. The junction capacitance is associated with oscillations in the depletion width due to small sinusoidal perturbations [41]. The diffusion capacitance is associated with minority carriers and changes in charge due to the sinusoidal perturbation signal. Because there is a distribution of trap and acceptor states within the irradiated silicon, the diffusion capacitance will not be a constant, but will itself be a function of frequency, and change the relationship between the complex impedance and frequency.

The equivalent series resistance of the device is dominated by the bulk resistivity of the silicon substrate. The range of this value is easily calculated. Resistance of a thin film is defined by the equation:

$$R = \frac{\rho L}{wt} \quad (3)$$

where ρ is the film resistivity, L is the length of the surface, w is the width of the surface (consider L the longer of the two values), and t is the film thickness perpendicular to the surface. Though dimensionless, the ratio L/W is taken as the number of squares through which charge carriers must traverse. A 380 μm thick substrate, with a 2 mm diameter contact (approximating $L/W = 1$ square) and resistivity between 1 and 10 $\Omega \times \text{cm}$ results in a resistance between 26 and 260 Ω . As previously stated, the equivalent series resistance parameter R3 does not deviate from this range, and changes in R3 are not considered to be a result

of irradiation, but rather small changes in carrier concentration within the silicon substrate, or small changes in device preparation.

R1 is the variable that undergoes the most drastic change. According to Nordell *et al.* [50], the resistivity of a-B₁₀C_{2+x}:H_y films ranges from 10¹⁰ to 10¹⁵ Ω×cm. A 200 nm thick film with a 2 mm diameter metal contact (approximating $L/W = 1$ square) would result in a resistance on the magnitude of 10¹⁶ Ω, 11 orders of magnitude greater than any resistance values obtained in Table 1. However, if the film is completely depleted of charge carriers, and only acting as a dielectric between 2 parallel plate contacts with a significant barrier at the silicon interface due to the heterojunction band misalignment, the values of R1 for the virgin and 0.1 dpa measurements can be explained.

First, it has yet to be shown what metals makes an ohmic contact with a-B₁₀C_{2+x}:H_y films. It is possible a metal with a higher work function than chromium is required. This suggests that there could be a contact resistance at the device cathode in the form of a Schottky barrier. However, since the Schottky barrier is a majority carrier process, the barrier is frequency independent, and will only change as a result of chemical or structural changes in the film. The band misalignment between the a-B₁₀C_{2+x}:H_y film and the silicon provides a frequency dependent junction resistance that will change as a result of changes in the charge carrier concentrations of either the film or the silicon.

Examining the virgin measurement, we first make the approximation from the indicated parallel resistance of 6082 Ω, that the a-B₁₀C_{2+x}:H_y film is fully depleted. Were this not the case, our calculation above shows that this value or the equivalent series resistance (R3) would be many orders of magnitude larger. This leads to the interpretation of this value as the junction resistance due to barriers within the band structure.

Examining the 0.1 dpa measurement, the second parallel R2 C2 component has an indicated junction resistance of 40 Ω [53]. Type inverted silicon as a result of neutron radiation reaches an upper limit asymptote of resistivity at approximately 2.4×10⁵ Ω×cm [51]. This is a direct result of the damage to the crystalline Si substrate. In order for the Si dopant to contribute to the conductivity of the Si, the substitutional atom (i.e. P) must sit on a Si lattice site. If the dopant is disturbed, and becomes an interstitial defect as a result of radiation damage, it is no longer active, and will not contribute to the conductivity. Prior to the damage clusters created near the ion end of range, the irradiating ion is creating point defects in the Si all along its ion track. These point defects reduce the average carrier relaxation time and de-activate the dopants, both of which increase the resistivity of the Si.

From equation (3), an ion range of 1400 nm and a contact area again of 2 mm diameter (approximating $L/W = 1$) would result in a resistance in the irradiated silicon of approximately 1.71×10⁹ Ω. However, as before this calculation assumes no depletion region, which is inaccurate. There will be a depletion region at the p-p⁺ junction with the a-B₁₀C_{2+x}:H_y/Si(irradiated), and at the p⁺-n homojunction between the Si(irradiated)/Si(virgin). Since neither the exact carrier concentration or change in band structure is known for the a-B₁₀C_{2+x}:H_y film, the depletion widths at this junction are not

accurately calculable. However, a rough estimate of the depletion width resulting from the p⁺-n homojunction shows the irradiated silicon and a-B₁₀C_{2+x}:H_y film being fully depleted. Just as with the examination of the a-B₁₀C_{2+x}:H_y film, a resistance on this order of magnitude is not found in the 0.1 dpa model, and lends support to the full depletion approximation.

Croitoru *et al.* [51] provide resistivity and mobility measurements of irradiated silicon, allowing for the calculation of the hole carrier concentration for the case $N_A \gg N_D$ through:

$$\rho = \frac{1}{q\mu_p N_A} \quad (4)$$

where ρ is resistivity, q is the elementary charge, μ_p is the hole hall mobility, and N_A is the acceptor concentration. Taking the values from Croitoru's highest measured fluences (10¹⁶ n/cm²) of $\rho = 234280$ Ω×cm and $\mu_p = 70$ cm²/Vs, we calculate $N_A = 3.8 \times 10^{11}$ 1/cm³. The carrier concentration of the virgin silicon substrate is estimated at $N_D = 1 \times 10^{15}$ 1/cm³ (based on the manufacturer's specifications). This leads to an estimate of the silicon homojunction depletion width (w) of 36 μm:

$$w = \left(\frac{2k_s \epsilon_0}{q} \left(\frac{N_A + N_D}{N_A N_D} \right) V_{bi} \right)^{1/2} \quad (5)$$

$$V_{bi} = \frac{kT}{q} \ln \left(\frac{N_A N_D}{n_i^2} \right) \quad (6)$$

where k_s is the dielectric constant, ϵ_0 is the permeability of free space, N_A is the number of acceptors, N_D is the number of donors, V_{bi} is the built in voltage, n_i is the intrinsic carrier concentration, k is the Boltzmann constant, T is temperature. Considering that the ion range is only 1.4 μm, and the a-B₁₀C_{2+x}:H_y film is only 225 nm thick, we can safely assume that the type-inverted silicon and a-B₁₀C_{2+x}:H_y film are fully depleted.

Of much more import in the 0.1 dpa data, is the decrease of R1 from 6028 to 2782 Ω. Using the approximation that the film is fully depleted of charge carriers, and the band alignment of the a-B₁₀C_{2+x}:H_y film to type inverted silicon is considered, the barrier of a p-p⁺ heterojunction will be much smaller than that of a p-n heterojunction even if the constituent band gaps are altered as a result of the irradiation. As an example to prove this point, let us assume the HOMO – LUMO gap of a-B₁₀C_{2+x}:H_y is 2.0 eV (values of 0.7 to 3.8 eV have been reported [40]). It has been shown that the acceptor and trap energy levels of type-inverted silicon are mid-band gap [55], so let us further assume that the band gap of the silicon is not significantly altered from 1.12 eV. The conduction band barrier of the a-B₁₀C_{2+x}:H_y/virgin silicon p-n heterojunction is roughly 2.0 eV – (E_f + E_{cN}) – (E_{vP} + E_f) eV ≈ 2.0 eV. Through band realignment of a type-inverted silicon region, the p-p⁺ conduction band barrier will be roughly 2.0 eV – 1.12 eV ≈ 0.88 eV. Such a reduction in the barrier height would be reflected in the parallel junction resistance component of our equivalent circuit model. Our example shows a reduction of roughly ½ in barrier height, which compares to our R1 results in Table 1.

Examination of the 0.2, 0.3, and 0.5 dpa measurements shows a dramatic increase in the resistance parameter R1 from 2782 to

190000 Ω . Maintaining the assumption that this remains a combination of the junction and contact resistances, one explanation for the dramatic increase of parameter R1 is further heterojunction band modification and/or Schottky barrier modification. This modification could be additional band realignment due to defect passivation resulting in a decrease in N_A and a shift from a p-type to an intrinsic semiconductor and simultaneously reducing the concentration of recombination/generation centers within the HOMO – LUMO gap. Another possibility is a direct change in the a-B₁₀C_{2+x}:H_y toward a larger HOMO – LUMO gap.

Previous work [24] showed improved diode rectification for 0.1 and 0.2 dpa irradiated samples through current – voltage $I(V)$ measurements (shown in Appendix A). Explanations thus far introduced do not account for these findings, meaning an additional mechanism must be at work. Supposition within [24] was that initial radiation passivated defects of discrete energy levels within the a-B₁₀C_{2+x}:H_y film. Defect passivation could result from electronic energy deposition, bond breaking and reformation of the local bonds with a lower total free energy, possibly resolving distorted icosahedron anion states. The low frequency conductance ($G_0 = dI/dV$), taken as $f < 100$ Hz, has a decreasing trend above 0.1 dpa. This would be reflected in a decrease in recombination/generation centers within the diode. The most likely place to look for this is within the a-B₁₀C_{2+x}:H_y film, as it has been shown that new mid-band gap vacancy complexes are forming in the silicon [43-49].

V. CONCLUSIONS

In conclusion, a-B₁₀C_{2+x}:H_y on Si p-n heterojunctions were synthesized utilizing PECVD. Following irradiation with 200 keV He⁺ ions, the heterojunction properties were explored through electrical characterization. A model has been presented for calculating conductance as a function of frequency for semiconductors under irradiation. This model was then used to interpret measured data and infer physical and chemical changes in the device.

For low doses of irradiation, the resistance of the R1 component decreased. This is most likely due to band realignment of the a-B₁₀C_{2+x}:H_y/Si heterojunction as the irradiated silicon type-inverts creating a p-p⁺ heterojunction and reducing the barrier height. Simultaneously, the crystalline Si substrate is being damaged. Point defects are decreasing the average carrier relaxation time, and dopants are being deactivated, resulting in an increase in the resistivity of the Si. For moderate doses of irradiation, it is believed that the electronic energy deposition from the irradiating ions may be perturbing the atoms within the a-B₁₀C_{2+x}:H_y film allowing for the elimination of defects, and decreasing the hole concentration (N_A). Even though the a-B₁₀C_{2+x}:H_y film is fully depleted of charge carriers, changes to the defect concentration (i.e. concentration of generation/recombination centers), and hole concentration (N_A) will change the Fermi energy (E_F) location within the HOMO-LUMO gap. This in turn causes band realignment, and would change the energy barrier at the a-B₁₀C_{2+x}:H_y/Si junction. Therefore, if the a-B₁₀C_{2+x}:H_y film has been altered to have less recombination/generation centers and/or smaller N_A the a-B₁₀C_{2+x}:H_y/Si junction resistance will increase, explaining the results of R1 in table 1.

While this paper presents a possible explanation for the initial increase in heterojunction device performance under irradiation, it is still not entirely clear to what extent the a-B₁₀C_{2+x}:H_y film is chemically or structurally modified by the irradiating ions. A more direct means of investigating the a-B₁₀C_{2+x}:H_y film is required. Future experiments seek to examine a-B₁₀C_{2+x}:H_y films as a lossy capacitor in a metal oxide semiconductor system (C-MOS). This will allow for the elimination of the issues created by the changing silicon substrate and exclusively examine the charge carriers of the a-B₁₀C_{2+x}:H_y film.

APPENDIX A

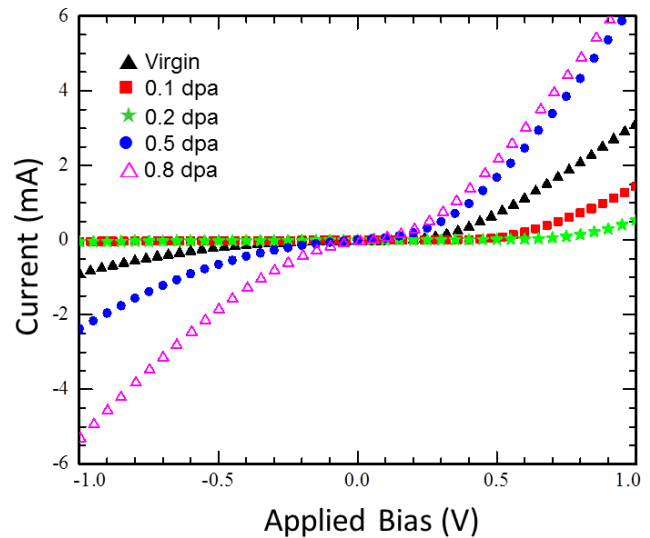


Fig. A1: Current vs. Voltage curves of a-B₁₀C_{2+x}:H_y on Si heterojunctions. The ‘▲’ represents the measured virgin data. The ‘■’ represents the measured 0.1 dpa data. The ‘★’ represents the measured 0.2 dpa data. The ‘●’ represents the measured 0.3 dpa data. The ‘△’ represents the measured 0.5 dpa data. This figure is reprinted with permission under License Number 3961511243923 [24].

APPENDIX B

Recognizing that the complex impedance of a resistor and capacitor in parallel is

$$Z_{R1C1} = \frac{R1(j\omega C1)^{-1}}{R1+(j\omega C1)^{-1}} \quad (B.1)$$

The equivalent complex impedance of the circuit in Fig. 1 is

$$Z_{eq} = -\frac{R1 j}{C1 \omega \left(R1 - \frac{j}{C1 \omega}\right)} - \frac{R2 j}{C2 \omega \left(R2 - \frac{j}{C2 \omega}\right)} + R3 \quad (B.2)$$

The complex admittance (Y) is the reciprocal of the complex impedance

$$Y = \frac{1}{Z_{eq}} = \left(\frac{-1}{\frac{R1 j}{C1 R1 \omega - j} + \frac{R2 j}{C2 R2 \omega - j} - R3} \right) \quad (B.3)$$

The conductance of a device is the real part of the complex admittance. To obtain the real component of Y , normalize the

equation

$$Y = -(C1 R1 \omega - j)(C2 R2 \omega - j) / [(R1 + R2 + R3 + (C2 R2 R3 \omega j) + (C2 R1 R2 \omega j) - (C1 C2 R1 R2 R3 \omega^2) + (C1 R1 R2 \omega j) + (C1 R1 R3 \omega j)] \quad (B.4)$$

Multiply by the complex conjugate

$$Y = -\frac{(C1 C2 R1 R2 \omega^2 - 1)\sigma_3}{\sigma_1} + \frac{(C1 R1 \omega + C2 R2 \omega)\sigma_2}{\sigma_1} + \left(\frac{(C1 R1 \omega + C2 R2 \omega)\sigma_3}{\sigma_1} + \frac{(C1 C2 R1 R2 \omega^2 - 1)\sigma_2}{\sigma_1}\right)j \quad (B.5)$$

where

$$\begin{aligned} \sigma_1 &= \sigma_2^2 + \sigma_3^2 \\ \sigma_2 &= C1 R1 R3 \omega + C2 R2 R3 \omega + C1 R1 R2 \omega + R1 R2 C2 \omega \\ \sigma_3 &= R1 + R2 + R3 - C1 R1 C2 R2 R3 \omega^2 \end{aligned}$$

Taking the real part of equation (B.5) gives the equation modeling the measured conductance

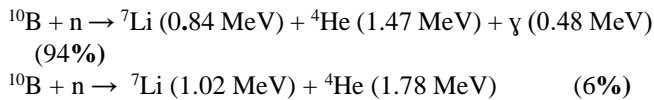
$$G_m = \frac{\omega^2((C1 R1 R2 + C2 R1 R2)(C1 R1 + C2 R2) + R3(C1 R1 + C2 R2)^2)}{(C1 C2 R1 R2 \omega^2 - 1)(-C1 C2 R1 R2 R3 \omega^2 + R1 + R2 + R3)} - \frac{\sigma_4}{\sigma_4} \quad (B.6)$$

where

$$\begin{aligned} \sigma_4 &= (C1 R1 R3 \omega + C2 R2 R3 \omega + C1 R1 R2 \omega \\ &\quad + C2 R1 R2 \omega)^2 \\ &\quad + (-C1 C2 R1 R2 R3 \omega^2 + R1 + R2 \\ &\quad + R3)^2 \end{aligned}$$

APPENDIX C

When a ^{10}B atom captures a neutron, a ^{11}B compound nucleus forms which fragments into ^7Li and an alpha particle with large translational energy, and 94% of the time, gamma radiation. This is represented below [1,10,34].



ACKNOWLEDGMENT

We would like to thank M. Chicoine of Université de Montréal for his contribution in obtaining the Elastic Recoil Detection data. We would also like to acknowledge S. Ducharme of the Department of Physics and Astronomy at the University of Nebraska – Lincoln for allowing the use of his laboratory's impedance analyzer. This work is partially supported by the Center for Integrated Nanotechnologies, a DOE Nanoscience user facility jointly operated by Los Alamos and Sandia National laboratories.

REFERENCES

- [1] A. N. Caruso, "The physics of solid-state neutron detector materials and geometries," *J. Phys. Condens. Matter*, vol. 22, no. 44, p. 443201, Oct. 2010.
- [2] A. N. Caruso, R. B. Billa, S. Balaz, J. I. Brand, and P. A. Dowben, "The heteroisomeric diode," *J. Phys. Condens. Matter*, vol. 16, no. 10, pp. L139–L146, Mar. 2004.
- [3] B. W. Robertson, S. Adenwalla, A. Harken, P. Welsch, J. I. Brand, P. Dowben, and J. P. Claassen, "A class of boron-rich solid-state neutron detectors," *Appl. Phys. Lett.*, vol. 80, no. 19, pp. 1344–3646, May 2002.
- [4] B. W. Robertson, S. Adenwalla, A. Harken, P. Welsch, J. I. Brand, J. P. Claassen, N. M. Boag, and P. A. Dowben, "Semiconducting boron-rich neutron detectors," in *Proc. SPIE*, 2002, vol. 4785, pp. 226–233.
- [5] S. Adenwalla, R. Billa, J. I. Brand, E. Day, M. J. Diaz, A. Harken, A. McMullen-Gunn, R. Padmanabhan, and B. W. Robertson, "Semiconducting boron-rich neutron detectors," in *Proc. SPIE*, 2004, vol. 5199, pp. 70–74.
- [6] K. Osberg, N. Schemm, S. Balkir, J. I. Brand, S. Hallbeck, and P. A. Dowben, "A hand-held neutron detection sensor system," in *Peter Dowben Publications*, 2006, vol. 112, p. 4 pp.
- [7] K. Osberg, N. Schemm, S. Balkir, J. I. Brand, M. S. Hallbeck, P. A. Dowben, and M. W. Hoffman, "A Handheld Neutron-Detection Sensor System Utilizing a New Class of Boron Carbide Diode," *IEEE Sens. J.*, vol. 6, no. 6, pp. 1531–1538, Dec. 2006.
- [8] A. N. Caruso, P. A. Dowben, S. Balkir, N. Schemm, K. Osberg, R. W. Fairchild, O. B. Flores, S. Balaz, A. D. Harken, B. W. Robertson, and J. I. Brand, "The all boron carbide diode neutron detector: Comparison with theory," *Mater. Sci. Eng. B*, vol. 135, no. 2, pp. 129–133, Nov. 2006.
- [9] E. Day, M. J. Diaz, and S. Adenwalla, "Effect of bias on neutron detection in thin semiconducting boron carbide films," *J. Phys. Appl. Phys.*, vol. 39, no. 14, p. 2920, Jul. 2006.
- [10] N. Hong, J. Mullins, K. Foreman, and S. Adenwalla, "Boron carbide based solid state neutron detectors: the effects of bias and time constant on detection efficiency," *J. Phys. Appl. Phys.*, vol. 43, no. 27, p. 275101, Jul. 2010.
- [11] N. Hong, L. Crow, and S. Adenwalla, "Time-of-flight neutron detection using PECVD grown boron carbide diode detector," *Nucl. Instrum. Methods Phys. Res. Sect. Accel. Spectrometers Detect. Assoc. Equip.*, vol. 708, pp. 19–23, Apr. 2013.
- [12] E. Echeverría, R. James, U. Chiluwal, F. L. Pasquale, J. A. C. Santana, R. Gapfizi, J.-D. Tae, M. S. Driver, A. Enders, J. A. Kelber, and P. A. Dowben, "Novel semiconducting boron carbide/pyridine polymers for neutron detection at zero bias," *Appl. Phys. A*, vol. 118, no. 1, pp. 113–118, Sep. 2014.
- [13] Ruqiang Bao, Zijie Yan, and D. B. Chrisey, "Charge carrier lifetime in boron carbide thin films," *Appl. Phys. Lett.*, vol. 98, no. 19, p. 192106, May 2011.
- [14] E. Echeverría, R. James, F. L. Pasquale, J. A. Colón Santana, M. S. Driver, A. Enders, J. A. Kelber, and P. A.

- Dowben, "Neutron Detection Signatures at Zero Bias in Novel Semiconducting Boron Carbide/Pyridine Polymers," in *Symposium DD/WW – Materials and Radiation Effects for Advanced Nuclear Technologies*, 2015, vol. 1743.
- [15] D. Simeone, C. Mallet, P. Dubuisson, G. Baldinozzi, C. Gervais, and J. Maquet, "Study of boron carbide evolution under neutron irradiation by Raman spectroscopy," *J. Nucl. Mater.*, vol. 277, no. 1, pp. 1–10, Jan. 2000.
- [16] A. Jostsons, C. K. H. DuBose, G. L. Copeland, and J. O. Stiegler, "Defect structure of neutron irradiated boron carbide," *J. Nucl. Mater.*, vol. 49, no. 2, pp. 136–150, Dec. 1973.
- [17] G. W. Hollenberg, B. Mastel, and J. A. Basmajian, "Effect of Irradiation Temperature on the Growth of Helium Bubbles in Boron Carbide," *J. Am. Ceram. Soc.*, vol. 63, no. 7–8, pp. 376–380, Jul. 1980.
- [18] G. W. Hollenberg and W. V. Cummings, "Effect of Fast Neutron Irradiation on the Structure of Boron Carbide," *J. Am. Ceram. Soc.*, vol. 60, no. 11–12, pp. 520–525, Nov. 1977.
- [19] T. Stoto, N. Housseau, L. Zuppiroli, and B. Kryger, "Swelling and microcracking of boron carbide subjected to fast neutron irradiations," *J. Appl. Phys.*, vol. 68, no. 7, pp. 3198–3206, Oct. 1990.
- [20] I. Caretti and I. Jiménez, "Point defects in hexagonal BN, BC₃ and BC_xN compounds studied by x-ray absorption near-edge structure," *J. Appl. Phys.*, vol. 110, no. 2, p. 023511, Jul. 2011.
- [21] A. Enyashin and A. Ivanovskii, "Structural, elastic, and electronic properties of icosahedral boron subcarbides (BC, BC₂), subnitride BN, and suboxide BO from data of SCC-DFTB calculations," *Phys. Solid State*, vol. 53, no. 8, pp. 1569–1574, Aug. 2011.
- [22] D. Emin, "Unusual properties of icosahedral boron-rich solids," *J. Solid State Chem.*, vol. 179, no. 9, pp. 2791–2798, Sep. 2006.
- [23] M. Carrard, D. Emin, and L. Zuppiroli, "Defect clustering and self-healing of electron-irradiated boron-rich solids," *Phys. Rev. B*, vol. 51, no. 17, pp. 11270–11274, May 1995.
- [24] G. Peterson, Q. Su, Y. Wang, P. A. Dowben, and M. Nastasi, "Improved p–n heterojunction device performance induced by irradiation in amorphous boron carbide films," *Mater. Sci. Eng. B*, vol. 202, pp. 25–30, Dec. 2015.
- [25] T. Maruyama, M. Iwanami, S. Ohnuki, T. Suda, S. Watanabe, and K. Ikezawa, "Precipitation and Amorphization in Boron Carbide Irradiated by High Energy Helium Ions," in *Effects of Radiation on Materials: 21st International Symposium*, M. Grossbeck, T. Allen, R. Lott, and A. Kumar, Eds. 100 Barr Harbor Drive, PO Box C700, West Conshohocken, PA 19428-2959: ASTM International, 2004, pp. 670–670–10.
- [26] C. Höglund, K. Zeitelhack, P. Kudejova, J. Jensen, G. Greczynski, J. Lu, L. Hultman, J. Birch, and R. Hall-Wilton, "Stability of 10B4C thin films under neutron radiation," *Radiat. Phys. Chem.*, vol. 113, pp. 14–19, Aug. 2015.
- [27] A. Aitkaliyeva, M. C. McCarthy, H.-K. Jeong, and L. Shao, "Irradiation studies on carbon nanotube-reinforced boron carbide," *Nucl. Instrum. Methods Phys. Res. Sect. B Beam Interact. Mater. At.*, vol. 272, pp. 249–252, Feb. 2012.
- [28] M. W. Mortensen, P. G. Sørensen, O. Björkdahl, M. R. Jensen, H. J. G. Gundersen, and T. Bjørnholm, "Preparation and characterization of Boron carbide nanoparticles for use as a novel agent in T cell-guided boron neutron capture therapy," *Appl. Radiat. Isot. Data Instrum. Methods Use Agric. Ind. Med.*, vol. 64, no. 3, pp. 315–324, Mar. 2006.
- [29] G. Victor, Y. Pison, N. Béreard, N. Toulhoat, N. Moncoffre, N. Djourelou, S. Miro, J. Baillet, N. Pradeilles, O. Rapaud, A. Maître, and D. Gosset, "Structural modifications induced by ion irradiation and temperature in boron carbide B₄C," *Nucl. Instrum. Methods Phys. Res. Sect. B Beam Interact. Mater. At.*
- [30] G. Nowak, M. Störmer, H.-W. Becker, C. Horstmann, R. Kampmann, D. Höche, M. Haese-Seiller, J.-F. Moulin, M. Pomm, C. Randau, U. Lorenz, R. Hall-Wilton, M. Müller, and A. Schreyer, "Boron carbide coatings for neutron detection probed by x-rays, ions, and neutrons to determine thin film quality," *J. Appl. Phys.*, vol. 117, no. 3, p. 034901, Jan. 2015.
- [31] B. Todorović-Marković, I. Draganić, D. Vasiljević-Radović, N. Romčević, M. Romčević, M. Dramićanin, and Z. Marković, "Synthesis of amorphous boron carbide by single and multiple charged boron ions bombardment of fullerene thin films," *Appl. Surf. Sci.*, vol. 253, no. 8, pp. 4029–4035, Feb. 2007.
- [32] M. M. Abdul-Gader, U. A. Al-Binni, A. A. Ahmad, M. A. Al-Basha, and N. J. Ianno, "Low-field current transport mechanisms in rf magnetron sputter deposited boron carbide (B₅C)/p-type crystalline silicon junctions in the dark," *Int. J. Electron.*, vol. 88, no. 8, pp. 873–901, 2001.
- [33] B. J. Nordell, C. L. Keck, T. D. Nguyen, A. N. Caruso, S. S. Purohit, W. A. Lanford, D. Dutta, D. Gidley, P. Henry, S. W. King, and M. M. Paquette, "Tuning the Properties of a Complex Disordered Material: Full Factorial Investigation of RECVD Grown Amorphous Hydrogenated Boron Carbide," *Mater. Chem. Phys.*, 2016.
- [34] G. F. Knoll, *Radiation Detection and Measurement*, 3rd ed. New York: Wiley, 2000.
- [35] M. Nastasi and J. W. Mayer, *Ion Implantation and Synthesis of Materials*. Springer, 2006.
- [36] G. W. Trucks, K. Raghavachari, G. S. Higashi, and Y. J. Chabal, "Mechanism of HF etching of silicon surfaces: A theoretical understanding of hydrogen passivation," *Phys. Rev. Lett.*, vol. 65, no. 4, pp. 504–507, Jul. 1990.
- [37] N. Hong, "An Exploration of Neutron Detection in Semiconducting Boron Carbide," University of Nebraska - Lincoln, Lincoln, NE, 2012.
- [38] M. S. Driver, M. M. Paquette, S. Karki, B. J. Nordell, and A. N. Caruso, "The electronic and chemical structure of the a-B₃CO_{0.5}:Hy-to-metal interface from photoemission spectroscopy: implications for Schottky

- barrier heights,” *J. Phys. Condens. Matter*, vol. 24, no. 44, p. 445001, Nov. 2012.
- [39] C. Pallier, J.-M. Leyssale, L. A. Truflandier, A. T. Bui, P. Weisbecker, C. Gervais, H. E. Fischer, F. Sirotti, F. Teyssandier, and G. Chollon, “Structure of an Amorphous Boron Carbide Film: An Experimental and Computational Approach,” *Chem. Mater.*, vol. 25, no. 13, pp. 2618–2629, Jul. 2013.
- [40] E. Echeverría, B. Dong, G. Peterson, J. P. Silva, E. R. Wilson, M. S. Driver, Y.-S. Jun, G. D. Stucky, S. Knight, T. Hoffman, Z. K. Han, N. Shao, Y. Gao, W.-N. Mei, M. Nastasi, P. A. Dowben, and J. A. Kelber, “Semiconducting Boron Carbides with Better Charge Extraction,” *Manuscr. Prep.*, 2016.
- [41] S. S. Li, “p-n Junction Diodes,” in *Semiconductor Physical Electronics*, S. S. Li, Ed. Springer New York, 2006, pp. 334–380.
- [42] R. Bao and D. B. Chrisey, “Short range order structure of amorphous B₄C boron carbide thin films,” *J. Mater. Sci.*, vol. 46, no. 11, pp. 3952–3959, Jun. 2011.
- [43] K. Gill, G. Hall, and B. MacEvoy, “Bulk damage effects in irradiated silicon detectors due to clustered divacancies,” *J. Appl. Phys.*, vol. 82, no. 1, pp. 126–136, Jul. 1997.
- [44] K. Gill, G. Hall, S. Roe, S. Sotthibandhu, R. Wheadon, P. Giubellino, and L. Ramello, “Radiation damage by neutrons and protons to silicon detectors,” *Nucl. Instrum. Methods Phys. Res. Sect. Accel. Spectrometers Detect. Assoc. Equip.*, vol. 322, no. 2, pp. 177–188, Nov. 1992.
- [45] E. Fretwurst, H. Feick, M. Glaser, C. Gößling, E. H. M. Jeyne, and A. Hess, “Reverse annealing of the effective impurity concentration and long-term operational scenario for silicon detectors in future collider experiments,” *Nucl. Instrum. Methods Phys. Res. Sect. Accel. Spectrometers Detect. Assoc. Equip.*, 1994.
- [46] D. Pitzl, N. Cartiglia, B. Hubbard, D. Hutchinson, J. Leslie, K. O’Shaughnessy, W. Rowe, H. F.-W. Sadrozinski, A. Seiden, E. Spencer, H. J. Ziock, P. Ferguson, K. Holzschneider, and W. F. Sommer, “Type inversion in silicon detectors,” *Nucl. Instrum. Methods Phys. Res. Sect. Accel. Spectrometers Detect. Assoc. Equip.*, vol. 311, no. 1–2, pp. 98–104, Jan. 1992.
- [47] P. A. Aarnio, M. Huhtinen, M. Pimiä, K. Kaita, M. Laakso, A. Numminen, and P. Ryytty, “Damage observed in silicon diodes after low energy pion irradiation,” *Nucl. Instrum. Methods Phys. Res. Sect. Accel. Spectrometers Detect. Assoc. Equip.*, vol. 360, no. 3, pp. 521–531, Jun. 1995.
- [48] S. J. Bates, C. Furetta, M. Glaser, F. Lemeilleur, E. León-Florián, C. Gößling, B. Kaiser, A. Rolf, R. Wunstorff, H. Feick, E. Fretwurst, G. Lindström, M. Moll, G. Taylor, and A. Chilingarov, “Pion-induced damage in silicon detectors,” *Nucl. Instrum. Methods Phys. Res. Sect. Accel. Spectrometers Detect. Assoc. Equip.*, vol. 379, no. 1, pp. 116–123, Sep. 1996.
- [49] K. Riechmann, K. T. Knöpfle, and V. M. Pugatch, “Pion and proton induced radiation damage to silicon detectors,” *Nucl. Instrum. Methods Phys. Res. Sect. Accel. Spectrometers Detect. Assoc. Equip.*, vol. 377, no. 2–3, pp. 276–283, Aug. 1996.
- [50] B. J. Nordell, S. Karki, T. D. Nguyen, P. Rulis, A. N. Caruso, S. S. Purohit, H. Li, S. W. King, D. Dutta, D. Gidley, W. A. Lanford, and M. M. Paquette, “The influence of hydrogen on the chemical, mechanical, optical/electronic, and electrical transport properties of amorphous hydrogenated boron carbide,” *Journal of Applied Physics*, vol. 118, no. 3, p. 035703, Jul. 2015.
- [51] N. Croitoru, R. Dahan, P. G. Rancoita, M. Tattaggi, G. Rossi, and A. Seidman, “Study of resistivity and majority carrier concentration of silicon detectors damaged by neutron irradiation up to 1016 n/cm²,” *Nuclear Instruments and Methods in Physics Research Section B: Beam Interactions with Materials and Atoms*, vol. 124, no. 4, pp. 542–548, May 1997.
- [52] R. F. Pierret, *Semiconductor Device Fundamentals*, 2nd edition. Reading, Mass: Addison Wesley, 1996.
- [53] Kim, J. M. Beebe, Y. Jun, X.-Y. Zhu, and C. D. Frisbie, “Correlation between HOMO Alignment and Contact Resistance in Molecular Junctions: Aromatic Thiols versus Aromatic Isocyanides,” *J. Am. Chem. Soc.*, vol. 128, no. 15, pp. 4970–4971, Apr. 2006.
- [54] E. Borchini and M. Bruzzi, “Radiation damage in silicon detectors,” *Riv. Nuovo Cim.*, vol. 17, no. 11, pp. 1–63, Oct. 2007.
- [55] B. C. MacEvoy, G. Hall, and K. Gill, “Defect evolution in irradiated silicon detector material,” *Nuclear Instruments and Methods in Physics Research Section A: Accelerators, Spectrometers, Detectors and Associated Equipment*, vol. 374, no. 1, pp. 12–26, May 1996.